Article:
Nanayakkara, K.I.U., Liew, A. and Gilbert, M. (2023) Application of thrust layout optimization to masonry structures. Proceedings of the Royal Society A: Mathematical, Physical and Engineering Sciences, 479 (2273). 20230053. ISSN: 1364-5021

https://doi.org/10.1098/rspa.2023.0053

PROCEEDINGS A

royalsocietypublishing.org/journal/rspa

Research

Cite this article: Nanayakkara KIU, Liew A, Gilbert M. 2023 Application of thrust layout optimization to masonry structures. *Proc. R. Soc. A* **479**: 20230053. https://doi.org/10.1098/rspa.2023.0053

Received: 26 January 2023
Accepted: 20 April 2023

Subject Areas:
civil engineering, structural engineering

Keywords:
limit analysis, masonry, thrust line, optimization

Author for correspondence:
Matthew Gilbert
e-mail: m.gilbert@sheffield.ac.uk

Application of thrust layout optimization to masonry structures

K. Isuru U. Nanayakkara, Andrew Liew and Matthew Gilbert

Department of Civil and Structural Engineering, The University of Sheffield, Mappin Street, Sheffield, S1 3JD, UK

KIUN, 0000-0003-2630-7724; MG, 0000-0003-4633-2839

A new automated analysis procedure designed to overcome limitations of the traditional thrust line analysis method for masonry gravity structures is presented. The procedure, termed thrust layout optimization (TLO), is capable of automatically identifying admissible thrust lines in masonry gravity structures comprising general arrangements of masonry blocks. The procedure employs a modified truss layout optimization with transmissible loads formulation, which means that an initial thrust line layout does not need to be specified in advance. Highly visual output is generated, allowing areas where tensile strength has been implicitly assumed to be clearly identified, which is beyond the scope of traditional thrust line analysis. Also, sliding failures can be modelled without difficulty. Finally, examples are used to demonstrate the efficacy of the TLO procedure; these show that thrust line bifurcations can be automatically identified in problems involving openings, and that there is no need to estimate the ineffective area in buttress wall problems, both issues for the traditional thrust line analysis method.

1. Introduction

Traditional load-bearing masonry structures have been used for millennia in construction, ranging in scale from individual dwelling houses to viaducts and cathedrals. Many of these structures have considerable historic value, and, to ensure they remain safe and

THE ROYAL SOCIETY PUBLISHING

fit for purpose, effective assessment methods are required [1,2]. The current climate emergency is also leading to renewed interest in stone masonry as a low embodied carbon means of construction [3,4] and this also makes it important that these structures are not needlessly demolished and replaced, at considerable cost to the environment.

To confirm the stability of masonry gravity structures, thrust line methods have been used since at least the time of Poleni [5]. As first pointed out by Hooke [6], 'as hangs the flexible line, so but inverted will stand the rigid arch'. This suggests that if a line of thrust can be found that lies entirely within the thickness of a masonry arch then the structure will be stable (neglecting the possibility for sliding failure or material crushing). This observation led to the development of the thrust line method, which has also been widely used in design, perhaps most famously by Gaudi when designing the Colònia Güell church near Barcelona [5]. In this case, a geometrically complex physical cable-net model was constructed to ensure the network of supports, ribs and vaults forming the building were appropriately proportioned to ensure stability.

More recently, computer-based methods have been used to assess the stability of masonry constructions. Although finite-element analysis methods have proved popular in a wide range of engineering disciplines, traditional linear elastic finite-element analysis is of limited use in the case of traditional masonry gravity structures, principally due to the typically minimal tensile stresses that can safely be sustained by masonry materials. Conversely, nonlinear finite-element methods, although powerful, are generally too computationally expensive and demanding of operator expertise for routine use. Similarly, although discrete element [7] and non-smooth contact dynamics (NSCD) methods [8] can be applied to masonry problems, the iterative solution procedure and requirement for the use of small timesteps makes them comparatively computationally expensive when a static analysis is involved.

Thus limit analysis approaches have proved popular, principally due to their ability to rapidly and directly analyse the collapse limit state. Building on the work of Kooharian [9] and Heyman [10], Livesley [11] proposed a rigid block limit analysis method, later extended by workers such as Ferris & Tin-Loi [12], Orduna & Lourenco [13], Gilbert *et al.* [14] and Nodargi *et al.* [15] to treat problems involving non-associative sliding friction between blocks. Although usually used to identify instantaneous collapse mechanisms, rigid block analysis problems involving gross displacements can also be handled (e.g. [16,17]).

However, rigid block methods require a masonry construction to be split either into constituent units, of which there are usually many, or into macro-blocks (e.g. [18]) to approximately represent these. In the latter case, since failure planes must coincide with the interfaces between blocks, there is a danger of overestimating the stability of a given masonry construction when a number of physical units are represented by a single macro block. Also, particularly when treating complex geometries, it is not straightforward to infer a continuous line of thrust from the output—e.g. in the recent contribution by Iannuzzo *et al.* [17] the lines are discontinuous.

As an alternative to explicitly discretizing a masonry structure into constituent blocks, in recent years there has been a resurgence in interest in thrust line methods, now taking advantage of various computer-based implementations. Notably, building on work by O'Dwyer [19], Block & Ochsendorf [20] developed the thrust network analysis (TNA) procedure to provide a rapid means of analysing and designing three-dimensional vaulted masonry structures. Using TNA, the geometry of a predefined network of thrust lines is adjusted until a stable solution is found, in which the thrust lines lie entirely within the masonry. TNA can be used to evaluate the safety of masonry structures by computing a geometric safety factor, or, by considering limiting horizontal thrusts at the supports, a 'stability domain' that describes admissible stress states [21]. However, the dependence of the results obtained on the topology of the initially defined thrust network remains an issue.

However, the thrust line method, whether undertaken by hand or via computer, has a number of inherent limitations. For example, to enable the self-weight of masonry lying below a thrust-line to be mobilized (i.e. be effectively 'lifted up'), it is implicitly assumed that the masonry possesses a degree of tensile resistance, but this is not necessarily transparent to the user. Consequently, to

avoid non-conservative outcomes, an inclined crack may need to be introduced when modelling masonry buttresses [22–24], and results are also sensitive to the way in which the masonry is discretized into blocks [25], something that is not always obvious to users. Furthermore, the usual assumption that the masonry possesses unlimited friction capacity can lead to non-conservative predictions of stability; e.g. even though a line of thrust can be identified that fits entirely within the masonry, sliding failure at the head of a flying buttress may lead to premature failure [26,27]. Premature, friction-induced, failure may also arise in multi-ring arches [28]. Finally, when complex geometries are involved (e.g. consider a gothic cathedral), it is often necessary to analyse parts of the structure separately and to then combine these to check overall stability, a somewhat cumbersome process [22].

In this paper, a new computational means of identifying admissible thrust lines in masonry gravity structures is proposed to overcome the aforementioned issues. The proposed procedure takes advantage of powerful layout (or 'topology') optimization techniques that have already been successfully used to automate the so-called 'strut and tie' method of design for reinforced concrete structures, where the goal is to identify tensile and compressive force paths in deep beams and other elements, enabling efficient layouts of tensile reinforcement to be identified [29]. In a traditional unreinforced masonry structure the goal is somewhat different, with the priority being to identify compressive force paths, with self-weight effects handled appropriately. Topology optimization has been little used previously in the field of masonry structures, with a rare example being usage in [30] to identify regions of compression for use in subsequent nonlinear finite-element pushover analyses of masonry walls. In the present contribution, it will be shown that a formulation employing truss layout optimization [31,32], used in tandem with transmissible loads [33,34], can be built on to directly identify compressive force paths and to establish margins of safety. It will be shown that this requires the introduction of interfaces to represent weak masonry joints, thereby allowing both tensile and sliding failures to be modelled, as well as changes to the optimization objective function.

The present paper is organized as follows. In §2, the development of the thrust layout optimization (TLO) formulation is outlined, with this then applied to a wide range of example problems in §3; in §4, conclusions are drawn.

2. Thrust layout optimization method

(a) Standard ground structure layout optimization procedure

The standard 'ground structure' layout optimization method was originally developed to identify optimal (minimum volume) truss structures [31,32,35–37]. The process involves the steps of: (i) specifying a design domain and boundary conditions—i.e. loading and support conditions (figure 1*a*), (ii) positioning nodes across the design domain, then interlinking these with potential members to form a 'ground structure' (figure 1*b*), and (iii) using linear programming (LP) to find the optimal structure to carry the applied loads (figure 1*c*). (Note that the basic LO formulation may result in structures that are in unstable equilibrium with the applied loads, e.g. see the structure shown in figure 1*c*.)

In terms of mathematics, for a problem involving a ground structure comprising n nodes and m potential members, the associated underlying LP problem formulation that involves finding the minimum volume truss structure (or 'truss-like' flow of forces) can be written as follows:

$$\min_{\mathbf{a},\mathbf{q}} \quad V = \mathbf{l}^{\mathrm{T}}\mathbf{a}, \tag{2.1a}$$

$$\text{s.t.} \quad \mathbf{B}\mathbf{q} = \mathbf{f}, \tag{2.1b}$$

$$-\sigma_{\mathrm{c}}\mathbf{a} \le \mathbf{q} \le \sigma_{\mathrm{t}}\mathbf{a} \tag{2.1c}$$

$$\text{and} \quad \mathbf{a} \ge \mathbf{0}, \tag{2.1d}$$

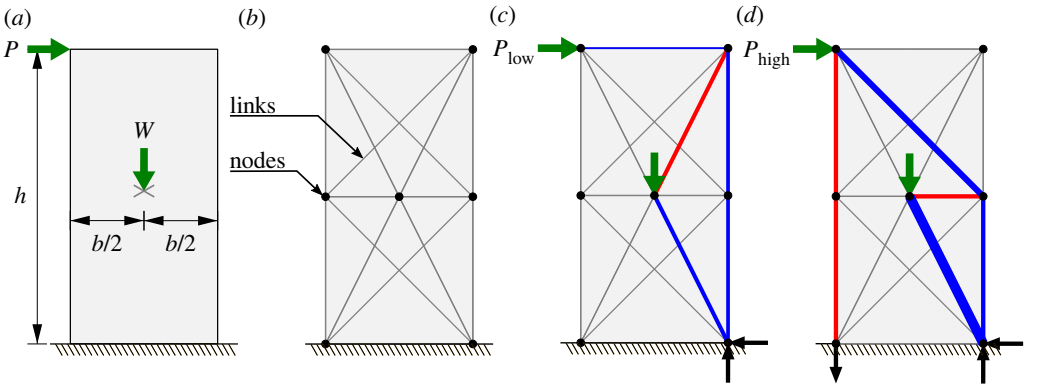

Figure 1. Standard 'ground structure' truss layout optimization (LO) procedure: (*a*) specified design domain, loading and support conditions; (*b*) nodes linked by potential members, creating a 'ground structure'; (*c*) optimal (minimum volume) layout identified by solving the underlying layout optimization problem; (*d*) optimal solution when a higher horizontal load is applied, involving the need for a support reaction that would be inadmissible if tension could not be transmitted to the support. Optimized truss layouts shown for values of P_{low}, P_{high}, W, h, b, σ_t and σ_c of 1, 2, 4, 2, 1, 1 and 100, respectively. Tension and compression forces shown in red and blue, respectively, with line thickness proportional to force magnitude.

where V is the volume of the truss structure; $\mathbf{l} = [l_1, l_2, \ldots, l_m]^T$ is a vector of ground structure member lengths and $\mathbf{a} = [a_1, a_2, \ldots, a_m]^T$ is a vector of member cross-sectional areas. Force equilibrium is imposed at nodes by equation (2.1*b*), where $\mathbf{B}$ is a $2n \times m$ matrix containing direction cosines, $\mathbf{q} = [q_1, q_2, \ldots, q_m]^T$ is a vector of internal member forces and $\mathbf{f} = [f_{1x}, f_{1y}, f_{2x}, f_{2y}, \ldots, f_{nx}, f_{ny}]^T$ is a vector of external applied loads. Yield constraints are enforced for each member by equation (2.1*c*), where σ_t and σ_c are limiting tensile and compressive stresses, respectively. Truss members are constrained to have zero or positive cross-sectional area in equation (2.1*d*). Since the objective function equation (2.1*a*) and all constraints are linear with respect to the optimization variables—member areas $\mathbf{a}$ and internal forces $\mathbf{q}$—this is therefore a LP problem that can be solved efficiently using modern LP solvers.

However, the problem set-up shown in figure 1 can alternatively be interpreted as a means of determining an admissible flow of forces in a loaded masonry gravity structure, here comprising a single stone block of height h, breadth b and weight W, resting on a rough horizontal base. In this case, the design domain in figure 1*a* now represents the extent of the block, with the self-weight of the block applied as a downward load W at its centre of mass. A horizontal external load P is applied at the top left corner. The generated minimum volume truss structure shown in figure 1*c* now corresponds to an admissible pattern of internal forces, where in this case the horizontal load P_{low} is (just) capable of overturning the block. Application of a larger horizontal load, P_{high}, corresponds to a solution involving support reactions that cannot be sustained by the masonry, assuming that the interface at the base of the block possesses zero tensile strength (figure 1*d*). This basic conceptual model will be developed further in subsequent sections of the present paper.

(b) Interface nodes representing weak masonry bonds

In the standard ground structure layout optimization solution shown in figure 1*d*, the node at the bottom left of the domain is supported and so can sustain an upward force; similarly the node at the bottom right of the domain can sustain a downward force. However, if the desire is to represent the stability of a stone block, as considered at the end of the previous section, the upward (tensile) force present at the left support cannot be sustained, assuming that the interface between the base of this block and the support cannot resist tension. To appropriately represent the required behaviour at block-to-block and block-to-support interfaces, interface nodes can now be introduced.

Interface nodes share the same physical location at a weak interface, but with each being associated with one of the adjacent blocks. This gives rise to node pairs that are each connected via a normal force q_n and a shear force q_s, respectively, aligned perpendicular and parallel to the interface. The weak interface is enforced by constraining the normal force to always be compressive, equation (2.2*b*), and the shear force to be limited by the normal force and friction coefficient between blocks at the interface, equation (2.2*c*).

To incorporate interfaces, equation (2.1) of the mathematical formulation is modified by replacing equation (2.1*b*) with the following equilibrium and yield constraints

$$\mathbf{Bq} + \mathbf{B_n q_n} + \mathbf{B_s q_s} = \mathbf{f}, \tag{2.2a}$$

$$\mathbf{q_n} \leq \mathbf{0} \tag{2.2b}$$

and

$$\mu \mathbf{q_n} \leq \mathbf{q_s} \leq -\mu \mathbf{q_n}, \tag{2.2c}$$

where in equation (2.2*a*) interface equilibrium matrices $\mathbf{B_n}$ and $\mathbf{B_s}$ are introduced, containing direction cosines on the basis of notional zero-length members oriented, respectively, perpendicular and parallel to the corresponding interface. Both matrices are of size $2n \times p$, where p is the number of interface node pairs. Also $\mathbf{q_n} = [q_{n,1}, q_{n,2}, \ldots, q_{n,p}]^{\mathrm{T}}$ is the interface normal force vector and $\mathbf{q_s} = [q_{s,1}, q_{s,2}, \ldots, q_{s,p}]^{\mathrm{T}}$ is the interface shear force vector. Finally, μ is the static friction coefficient for block-to-block and block-to-support interfaces.

(c) Transmissible self-weight loads

Returning to the example shown in figure 1, when this was interpreted as a single block gravity structure analysis problem, the self-weight of the block was assumed to be applied at the centre of mass, leading to somewhat convoluted patterns of internal forces being identified. However, when constructing a funicular polygon using the traditional thrust line method, self-weight loads are allowed to move along their lines of action, permitting identification of simpler, compression-only, patterns of internal forces. This is something that can be reproduced in layout optimization by the use of 'transmissible' loads [33,34,38]. These are loads that are shared across multiple nodes lying along a given vertical line of action when self-weight loads are involved.

To illustrate the concept, in figure 2*a*, the self-weight in the single stone block example is now modelled using two vertical strips of material. The self-weight of each strip can be considered as a transmissible load, with this shared between nodes lying along its line of action (figure 2*a*,*b*), as opposed to being fixed at its centre of mass (as in figure 1). As the number of strips (or transmissible load lines) is increased, it is evident that the solution will tend towards a traditional thrust line solution—see figure 2*c*, where here 25 transmissible load lines have been employed, with σ_t and σ_c set, respectively, to 1 and 100 to identify a thrust layout where compressive forces are dominant.

In comparison to constraint equation (2.1*b*), which was used when generating figure 1, introduction of transmissible self-weight loads w requires these to be separated from externally applied loads f in the equilibrium equation—see equation (2.3*a*) below. Also, the self-weight loading applied to a given node (denoted w) now needs to be represented by an optimization variable, with the total self-weight load associated with each transmissible load group ($\bar{w}$) fixed for a given discretization by constraint equation (2.3*b*). Finally, constraint equation (2.3*c*) is also needed in order to avoid spurious solutions from being identified (see [34] for an explanation of why this is necessary):

$$\mathbf{Bq} - \mathbf{w} = \mathbf{f}, \tag{2.3a}$$

$$\mathbf{H}\,\mathbf{w} = \bar{\mathbf{w}} \tag{2.3b}$$

and

$$\mathbf{w} \geq \mathbf{0}, \tag{2.3c}$$

where $\mathbf{w} = [0, w_1, 0, w_2, \ldots, 0, w_n]^{\mathrm{T}}$ is the nodal self-weight load vector. Note that as self-weight loads are applied in the vertical direction, only vertical equilibrium constraints are affected. Also,

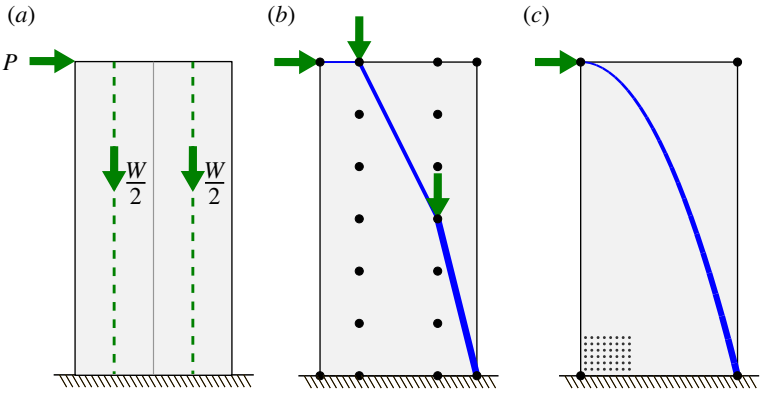

Figure 2. Including self-weight via transmissible loads: (*a*) discretization of the self-weight of a notional masonry block via two vertical strips; (*b*) positions of nodes along transmissible load lines and the resulting optimal force flow; (*c*) optimal force flow obtained using a finer resolution—with block self-weight now discretized via 25 transmissible load lines and using a post-processing geometry optimization rationalization step to improve clarity (after [39]).

$\bar{\mathbf{w}} = [\bar{w}_1, \bar{w}_2, \ldots, \bar{w}_g]^{\mathrm{T}}$ is the load group vector, where g is the number of transmissible self-weight load groups in the problem and $\bar{w}_i$ is the total load applied in transmissible load group i. Binary matrix $\mathbf{H}$ specifies which nodal load components in $\mathbf{w}$ belong to which load group in $\bar{\mathbf{w}}$, where $\mathbf{H}$ is of size $g \times 2n$ and is given by

$$\mathbf{H}_{ij} = \begin{cases} 1 & \text{if load component } j \text{ exists in load group } i \\ 0 & \text{otherwise.} \end{cases} . \tag{2.4}$$

(d) Proposed thrust layout optimization procedure

The developments described in the preceding sections provide the basic foundations for a new analysis method for masonry gravity structures, henceforth termed thrust layout optimization (TLO). The method builds on the standard ground structure truss layout optimization method by (i) introducing interface nodes to represent weak interfaces and (ii) representing self-weight loads as transmissible loads. However, several further developments are required to realize the TLO procedure; these include changes to the optimization objective function, and are described in this section.

As with the standard truss layout optimization procedure, TLO first requires that the extent of the problem domain and the nature of loading and boundary conditions are prescribed (figure 3*a*). However, in this case, the problem domain is bounded by the outline of the masonry gravity structure, and the presence of weak interfaces between blocks needs to be identified. Nodes are generated in both the interior and at boundaries of blocks, while interfaces are populated with interface nodes. Links are created between all nodes in the same block (figure 3*b*). These links, representing potential internal force paths, are allowed to take any compression force, but the maximum tensile force is limited by a value $q^{\mathrm{t}}_{\max}$, to reflect the non-zero, albeit usually relatively low, tensile strength of masonry blocks. Self-weight loading is applied as transmissible loads, with the line of action constrained to lie within any given block (figure 3*c*). This prevents the self-weight of a given block being 'lifted up' across a weak interface.

When assessing the stability of a masonry gravity structure, a common goal is to seek the magnitude of applied load that can be applied before collapse occurs. To achieve this, rather than seeking the minimum volume truss associated with equation (2.1), the objective of the optimization needs to be changed to one of finding the collapse load factor (the multiplier on a given load required to trigger failure). This can be achieved by maximizing the load factor subject to equilibrium and yield constraints, using the defined ground structure and set of transmissible

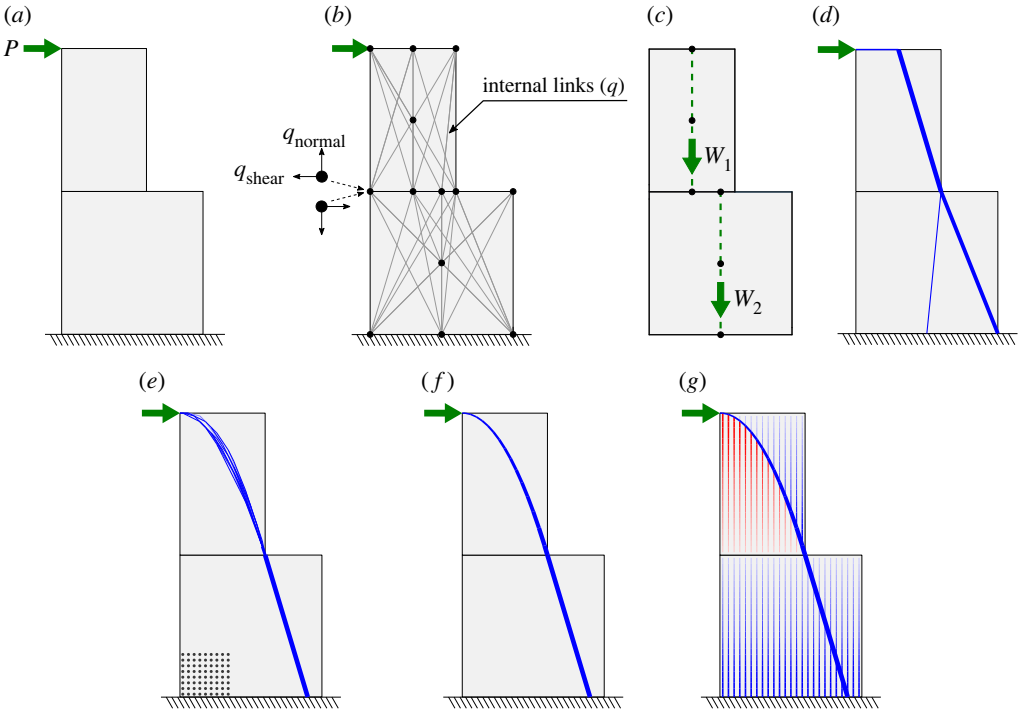

Figure 3. Application of proposed thrust layout optimization (TLO) procedure to a simple two block problem: (*a*) geometry of blocks and location of external load *P* and support; (*b*) problem discretized via nodes and links; (*c*) masonry self-weight represented by transmissible loads W_1 and W_2; (*d*) collapse load and thrust layout found by solving the associated layout optimization problem; (*e*) thrust layout obtained when using a finer resolution nodal grid (as indicated); (*f*) thrust layout obtained after also performing a post-processing geometry optimization rationalization step, and (*g*) layout with transmissible self-weight vectors also plotted—compression and tensile transmissible self-weight vectors are shown in blue and red respectively, with line thicknesses representing the magnitude of the forces.

self-weight loads created—resulting in the modified formulation given in equation (2.5) below:

$$\max_{\mathbf{q},\mathbf{q_n},\mathbf{q_s},\mathbf{w},\lambda} \quad \lambda, \tag{2.5a}$$

$$\text{s.t.} \quad \mathbf{B}\mathbf{q} + \mathbf{B_n}\mathbf{q_n} + \mathbf{B_s}\mathbf{q_s} - \mathbf{w} - \boldsymbol{\lambda}\mathbf{f} = \mathbf{0}, \tag{2.5b}$$

$$\mathbf{H}\,\mathbf{w} = \bar{w}, \tag{2.5c}$$

$$\mathbf{q} \le q^{\mathrm{t}}_{\max}\mathbf{1}, \tag{2.5d}$$

$$\mathbf{q_n} \le \mathbf{0}, \tag{2.5e}$$

$$\mu\mathbf{q_n} \le \mathbf{q_s} \le -\mu\mathbf{q_n}, \tag{2.5f}$$

$$\mathbf{w} \ge \mathbf{0} \tag{2.5g}$$

$$\text{and} \quad \boldsymbol{\lambda} \ge 0, \tag{2.5h}$$

where $\boldsymbol{\lambda}$ is the load factor on the externally applied loads, and other terms are as defined previously. Thus the factor on externally applied loads is maximized under the constraints of (i) static equilibrium at nodes—equations (2.5*b*) and (2.5*c*), (ii) a maximum tensile force allowed within blocks, equation (2.5*d*), with no tensile forces allowed across weak interfaces, equation (2.5*e*), and (iii) interface friction force limited by friction coefficient, equation (2.5*f*). The linear nature of the objective function and constraints means that the problem can be solved using LP.

Finally, although solving equation (2.5) will determine the collapse load factor, the associated solution may include spurious self-equilibriating force networks, since these are not explicitly penalized in equation (2.5). This will in turn lead to thrust layouts that are not visually clear. To address this, a volume minimization post-processing step can be performed, with the computed load factor constrained to lie at the value found in the load factor evaluation step. This is carried out using the basic layout optimization formulation presented in equation (2.1), with interface nodes, equation (2.2), and transmissible self-weights, equation (2.3), now also included in the model. Outcomes from the process are shown in (figure 3*d*,*e*). A further post-processing geometry optimization rationalization step (after [39]) can help further improve the visual clarity of the force flow; see figure 3*f*. Furthermore, in addition to the thrust lines obtained via the TLO process (shown in figure 3*d*,*e*,*f*), the vertical self-weight vectors hidden by the assumed transmissibility of self-weight loads can also be optionally plotted to provide additional visual information; see figure 3*g*. These transmissible self-weight vectors are force vectors indicating the force in the notional link required to move the self-weight either up or down from its original position to where it is transmitted to, the former requiring tensile links and the latter compressive links.

(e) Software implementation

To enable two-dimensional mesh geometries created in a CAD environment to be efficiently converted into an appropriate data structure for use with the developed TLO procedure, a suitable digital workflow was developed. Thus the software Rhinoceros [40] was used to prepare the presented examples, with an export process developed to transfer vertex and face data. The TLO procedure itself was implemented as a computational algorithm using the Python programming language [41], making use of the numerical package NumPy [42], geometry package Shapely [43] and LP solver MOSEK [44].

When working with problems involving large numbers of discrete blocks, it is important to employ a robust and efficient data structure for: (i) tracking connectivity between vertices, edges, faces and links, (ii) storing information on loads, degrees-of-freedom and internal forces as properties, (iii) performing efficient algorithmic operations and manipulations on the underlying geometry, and (iv) saving, loading and editing instances of the data structure through the optimization pipeline. Thus for data handling, a hybrid data structure was created to facilitate storing of information and performing operations on geometric data through vertices, edges, faces and links, where the links are the straight lines connecting vertices. Thus the general purpose open-source half-edge data structure OpenMesh [45] was used for the management of vertices, edges and faces, and NetworkX [46] was used for handling link connectivity.

(f) Verification of method

To verify the proposed method, two simple example problems are now considered: (i) a simple two block problem (figure 4); (ii) a semicircular arch problem (figure 5).

Considering first the two block problem shown in figure 4, this comprises a solid block stacked on a larger solid block. The stack of blocks is subjected to a horizontal point load at the top left corner as indicated. Two cases are considered: (i) assuming the interfaces possess infinite friction capacity (figure 4*a*,*b*), and (ii) that the friction coefficient at the interfaces is 0.25 (figure 4*c*,*d*). In the former case the failure load is found to be 18, with the top block overturning (figure 4*a*,*b*), while in the latter case the failure load is found to be 15, with the top block sliding (figure 4*c*,*d*).

The correctness of these values can be verified via simple analytical calculations or rigid block analysis software, confirming the ability of TLO to correctly determine the failure load for problems with or without frictional failure. Here, the LimitState:GEO software package [47], which implements the discontinuity layout optimization method [48,49], was used to perform the rigid block analysis calculations. For the overturning block case, the TLO thrust layout shows forces passing through the bottom right corner of the top block (figure 4*a*), coinciding with where the rigid block model indicates overturning failure of this block occurs (figure 4*b*). By contrast, in

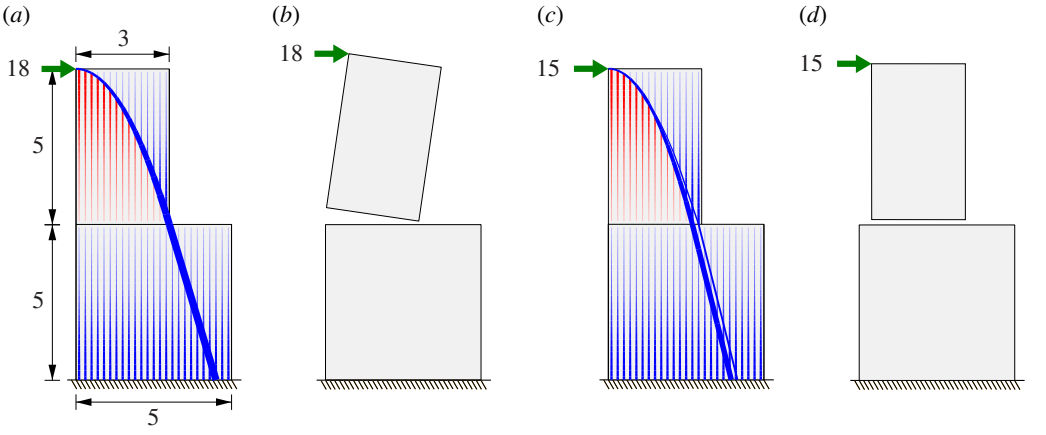

Figure 4. Two block problem—influence of friction: (*a*) TLO solution assuming infinite friction; (*b*) corresponding rigid block mechanism; (*c*) TLO solution assuming coefficient of friction of 0.25; (*d*) corresponding rigid block mechanism (blocks have width of 2 units and unit weight of 2 units; thrust layouts obtained using internal and boundary node spacings of 0.2 and 0.1 units, respectively; layouts then rationalized via geometry optimization post-processing step, with transmissible load vectors also plotted; rigid block solutions obtained independently using LimitState:GEO software [47]).

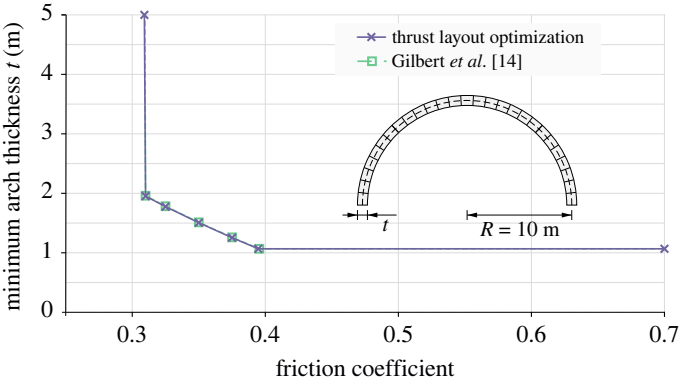

Figure 5. Semicircular arch problem: minimum arch thickness required for stability under self-weight for various coefficient of friction values, showing agreement between TLO results and those of Gilbert *et al.* [14] (arch contains 27 voussoirs).

the sliding block case (figure 4*c*), the thrust line bifurcates and spreads over a region at the block interface.

Considering next a semicircular arch with a centreline radius (R) of 10 m unit width and unit density. In this case, the minimum arch thickness t required to carry its self-weight can be determined for any given friction coefficient by trying a range of different arch thicknesses; results are shown in figure 5. For friction coefficients higher than 0.395, a minimum arch thickness ratio (t/R) of 10.68 % was obtained. This matches well with the minimum arch thickness ratio of 10.75 % obtained by Ocshendorf [23], assuming a continuum arch (the difference is because a continuum arch can fail at any radial plane whereas weak planes were here positioned between the 27 voussoirs assumed to form the arch). At friction coefficients smaller than 0.31, the minimum thickness required was found to rise rapidly as the arches undergo sliding failure. By contrast, at friction coefficients greater than 0.395 failure is due to hinging, with a mixed mode of sliding and hinging failure in the intermediate range. Across the full range of friction coefficients considered,

the results obtained using TLO were found to coincide perfectly with the numerical results obtained previously by Gilbert *et al.* [14].

(g) Commentary

In his seminal work Heyman [6] presented the funicular polygon (i.e. a graphical static construction of a hanging chain) as a line of thrust that could be used to check the safety of a masonry gravity structure; this has subsequently been widely adopted by practising engineers. However, more recently, it has been pointed out that the funicular polygon may not always represent a valid thrust line [25,50,51]. The issue stems from the fact that the arrangement of the interfaces, or joints, between blocks (termed the 'stereotomy') is not explicitly considered in the construction of a funicular polygon. Instead, as demonstrated in [25,52,53], a given arch or other structure is implicitly taken to be made up of a series of vertical strips of material. This is likely to lead to incorrect predicted collapse loads, as the importance of stereotomy on the latter has previously been demonstrated [51,54]. Furthermore, this may lead to situations where a self-weight load is inadvertently assumed to be transferred upwards across a weak interface, leading to an overestimated predicted load carrying capacity. By contrast, in the TLO procedure weak interfaces are explicitly considered, preventing this from occurring. Thus a thrust layout obtained by TLO can be viewed as a corrected thrust line solution, with the corresponding computed collapse load converging towards the exact limit load as the numerical discretization is refined. Also, in a TLO solution, the flow of the principal forces remains clearly evident, with, in the interests of transparency, transmissible self-weight loads also plottable if required.

Note that in the literature various means of constructing a thrust line are described, leading to differences in the form of the thrust line itself; see [51,55]. Here, a funicular polygon is used for this purpose (after Heyman [10]). Of the different forms of thrust line, the funicular polygon compares well with the thrust layouts described herein, with both providing a clear means of visualizing force-flows.

3. Examples

A selection of illustrative examples and applications are presented in this section to demonstrate the efficacy of the proposed TLO method. Results are compared with those from traditional thrust line and rigid block analysis methods. All computations were performed on a PC employing an Intel(R) Core(TM) i7-8700 processor running at 3.20 GHz under Microsoft Windows 10. A Python implementation of the TLO method has been made available to accompany the paper, along with detailed nodal coordinate and connectivity information for all the example problems described (see Data accessibility statement). The nodal spacings used to generate the thrust layouts presented were selected primarily to ensure visual clarity, given that the computed TLO collapse loads can be observed to be comparatively insensitive to the nodal spacing used, providing a reasonable number of nodes are used—see results from the parametric study conducted in the case of Example (iii), which involves a flat arch on stone columns. For the volume minimization post-processing step of the TLO runs a material strength ratio ($\sigma_t : \sigma_c$) of 1 : 100 was set to penalize the presence of tensile forces. For the range of material strength ratios typically observed for stone masonry, this has been observed to have little effect on the visualization, i.e. the locations of tension remain unaffected while the extent of the tension in these areas may vary slightly.

In the case of some examples, traditional thrust line solutions are also presented for comparative purposes. These are funicular polygons drawn at the point of incipient collapse, identified using custom written code written in MATLAB R2019b, taking advantage of its optimization toolbox. Rigid block models were also created for some examples; in this case the analyses were performed using the commercially available LimitState:GEO software package [47].

In the case of both the traditional thrust line solutions and the TLO solutions, compressive and tensile forces are plotted respectively using blue and red lines. In the case of the traditional

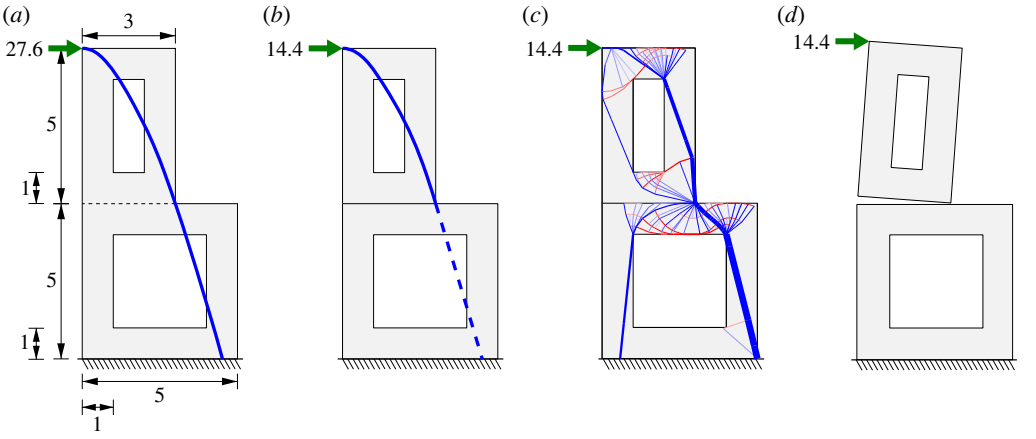

Figure 6. Stacked blocks with voids—solutions obtained via: (*a*) traditional thrust line method, assuming monolithic masonry; (*b*) traditional thrust line method, only considering upper block; (*c*) TLO, showing a force flow that is confined to areas where material is present; (*d*) rigid block analysis method, showing collapse mechanism only (blocks have width of 2 units and a unit weight of 2 units; thrust lines obtained using 0.2 unit wide vertical strips; thrust layouts obtained using internal and boundary node spacings of 0.2 units and $q^{t}_{max} = 0.005$; thrust layout rationalized via geometry optimization post-processing step; infinite friction assumed at interfaces between blocks; note that although the thrust lines in (*a*) and (*b*) are qualitatively similar, they are not identical).

thrust line solutions, thrust lines are plotted with uniform thickness while in the case of the TLO solutions the line thickness is varied to reflect the magnitude of the forces involved, scaled linearly from 0.05 at q_{min} to 1.0 at q_{max}. In the interests of visual clarity, forces q lower than q_{min} are not plotted, with q_{min} set as $0.001\,q_{max}$, and forces below $0.05\,q_{max}$ plotted in a progressively lighter colour shade. Finally, in the case of some TLO plots, transmissible load vectors are also plotted; in this case, the associated line thickness is scaled up by a factor of 5 relative to other force vectors to ensure these are visible. Finally, the post-processing geometry optimization rationalization step described in [39] is employed to improve visual clarity as required.

(a) Illustrative examples

Capabilities of the proposed TLO method are first explored via three illustrative examples, consisting of: (i) stacked blocks with voids, (ii) a segmental arch with and without voids, and (iii) a flat arch on stone columns.

(i) Stacked blocks with voids

This problem consists of two hollow blocks placed on top of each other, subjected to a horizontal force at the top left corner of the upper block, as shown in figure 6. The predicted collapse load and visual representation of internal forces obtained using TLO is compared with those obtainable using the traditional thrust line and rigid block methods.

Firstly, consider the traditional thrust line analysis solutions shown in figure 6*a*,*b*. These show thrust lines that pass through the internal void, with it not being clear whether these are admissible—given that Heyman's safe theorem [10] requires thrust lines to 'lie wholly within the masonry'. In the first thrust line solution (figure 6*a*), the stereotomy of blocks is not considered, leading to an unrealistically high collapse load estimate of 27.6 units. This arises from 'lifting up' of the lower block across the weak interface between blocks. When this weak interface is explicitly modelled, e.g. by only considering equilibrium of the upper block, the traditional thrust line method then yields a more realistic collapse load (of 14.4 units, figure 6*b*). This can be shown

to be the exact collapse load for this problem, and is also predicted by the TLO and rigid block methods (figure 6*c*,*d*, respectively).

Considering now the TLO solution (figure 6*c*), this explicitly respects block stereotomy (by including no-tension interfaces and allowing transmissibility of self-weight only within blocks), and also successfully identifies a force flow that remains entirely within the material volume, passing from the externally applied load through to the supports. The TLO solution also correctly indicates that some intrinsic tensile strength of the masonry block material needs to be mobilized. In comparison, although the rigid block limit analysis solution shown in figure 6*d* depicts the critical collapse mechanism, no information about the internal distribution of forces within the structure is provided.

(ii) Segmental arch

The next example involves two segmental arches composed of a number of equally sized voussoirs, one solid and one including three internal holes positioned on the arch centreline; see figure 7. Both arches are subjected to an offcentre point load, as indicated. To ensure no sliding failures occur, a friction coefficient of 1 is assumed.

Firstly, the traditional thrust lines shown in figure 7*a* and *b* both lie entirely within the masonry, not passing through the holes in the case of the structure shown in figure 7*b*. However, these correspond to very conservative estimates of collapse load (P of 39.8 kN for the solid arch and 27.6 kN for the arch with holes). By recognizing that the blocks do possess some tensile strength, the traditional no tension condition can instead be enforced only at interfaces between blocks, resulting in the thrust line solutions shown in figure 7*c* and *d*, which correspond to significantly higher collapse loads (P of 62.4 kN for the solid arch and 57.4 kN for the arch with holes). However, the thrust lines no longer lie entirely within the masonry, rendering the status of these solutions potentially unclear.

Considering now the corresponding TLO solutions, shown in figure 7*e* and *f*, the predicted collapse loads (P of 63.1 kN for the solid arch and 58.1 kN for the arch with holes) are similar to those obtained via thrust line analysis with the no tension condition enforced only at block interfaces[1], though force flows that remain entirely within the material volume are now clearly identified. Specifically, areas of the blocks where tensile strength is required are now evident (e.g. where the traditional thrust lines lie outside the thickness of the arch), and the bifurcation of the thrust line around one of the internal voids (figure 7*f*) now effectively verifies the reasonableness of allowing the traditional thrust line to pass through this (figure 7*d*). Thus TLO provides a new, and potentially extremely valuable, perspective on how forces flow in such structures. Finally, although the collapse loads predicted via rigid block limit analysis are the same as the TLO method (compare figure 7*e*,*f* with figure 7*g*,*h*), no information about the internal distribution of forces within the structure is provided when using this method.

(iii) Flat arch on stone columns

The next example, involving a flat arch supported by two stone columns, demonstrates that the collapse load predicted using the thrust line method can be significantly in error, even when the thrust line is constrained to lie within the thickness of the masonry only at interfaces. The structure is shown in figure 8 and is made up of five equally sized blocks, plus associated springing blocks. To ensure no sliding failures occur, a friction coefficient of 1 is assumed.

Firstly, a traditional thrust line analysis solution, with the thrust line lying entirely within the thickness of the masonry, is shown in figure 8*a*. However, while this solution appears qualitatively reasonable, it is evident that the associated collapse load is low, at $P = 10.1$ kN. When the thrust line is constrained only to lie within the thickness of the masonry at block interfaces, a higher associated collapse load, of $P = 16.2$ kN, is obtained, as shown in figure 8*c*. However, this is still

[1]The slight difference between the collapse loads predicted via traditional thrust line analysis (figure 7*c*,*d*) and TLO (figure 7*e*,*f*) is due to the thrust line analysis not considering block stereotomy, instead assuming the arches to be formed using notional vertical strips [25]. This issue is further explored in (iii), the flat arch on stone columns example.

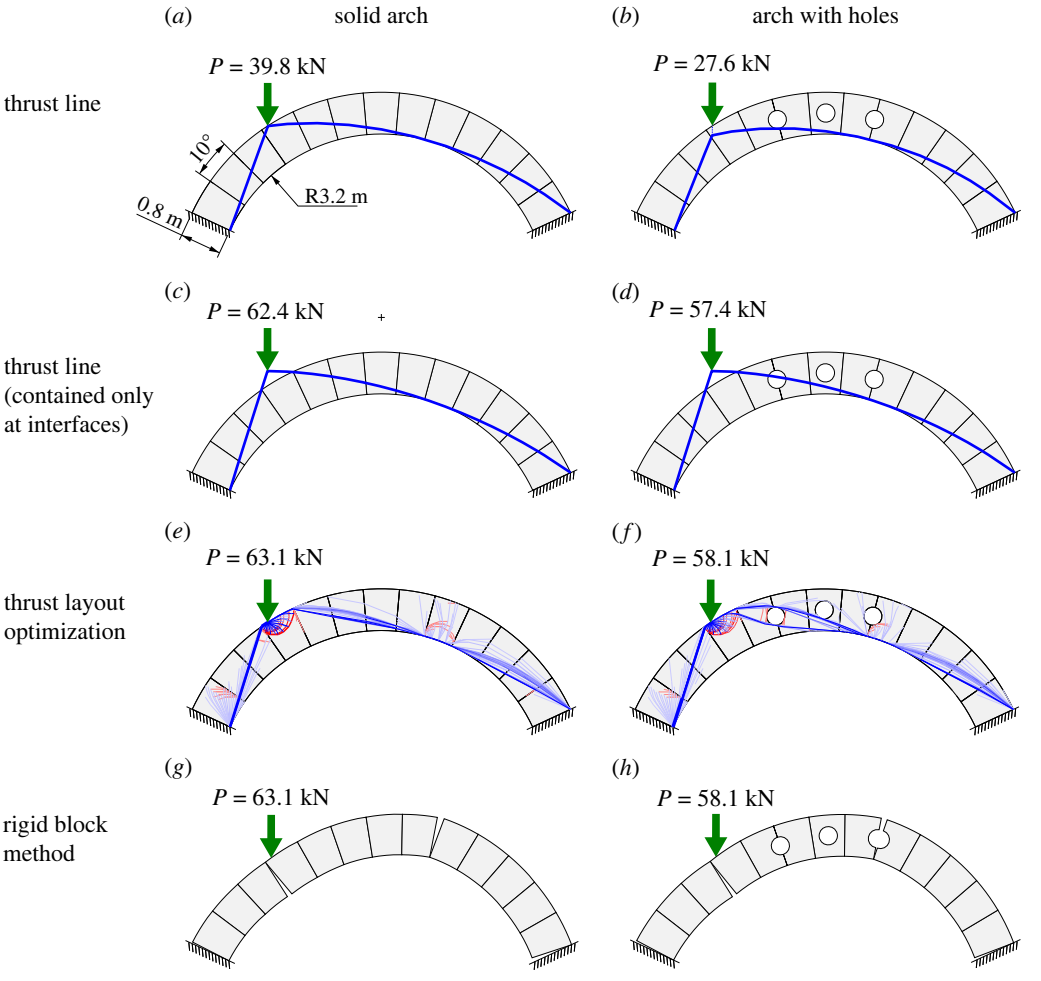

Figure 7. Segmental arch—solutions obtained via: (*a*,*b*) traditional thrust line method; (*c*,*d*) thrust line method with thrust constrained at block interfaces only; (*e*,*f*) TLO, showing force flows confined to areas where material is present; (*g*,*h*) rigid block method, showing collapse mechanisms only (arch span: 5.80 m, rise 1.85 m, width 0.1 m, unit weight: 25 kN m^{-3}; circular voids on arch centreline at locations indicated have diameter of 0.35 m; collapse load *P* in kN applied 0.72 m from left support; thrust lines obtained assuming self-weight lumped at block centroids; thrust layouts obtained using internal and boundary node spacings of 0.05 m and $q^{t}_{max} = 250$ N; thrust layout tensile force line thickness scaled by a factor of 2 for emphasis).

significantly lower than the predicted collapse load of $P = 45.1$ kN obtained when using TLO (figure 8*e*), with the correctness of this solution verified using the rigid block method (figure 8*f*). The discrepancy in computed collapse loads is a consequence of the thrust line solutions being represented by funicular polygons, derived by discretizing the structure using vertical strips of material [25], with here each strip having a width of 0.05 m. These solutions can be reproduced using the rigid block method by introducing vertical cracks at locations where the thrust line touches the edges of the masonry; thus the rigid block solution shown in figure 8*b* corresponds to the thrust line solution shown in figure 8*a*. Similarly, when the keystone crack is omitted, the rigid block solution shown in figure 8*d* is obtained, corresponding to the less constrained thrust line solution shown in figure 8*c*. (The collapse loads shown in figure 8*c*,*d* are not exactly the same—16.191 kN in (*c*) and 16.171 kN in (*d*), with the small difference being due to the two sides of the keystone block being slightly off-vertical.)

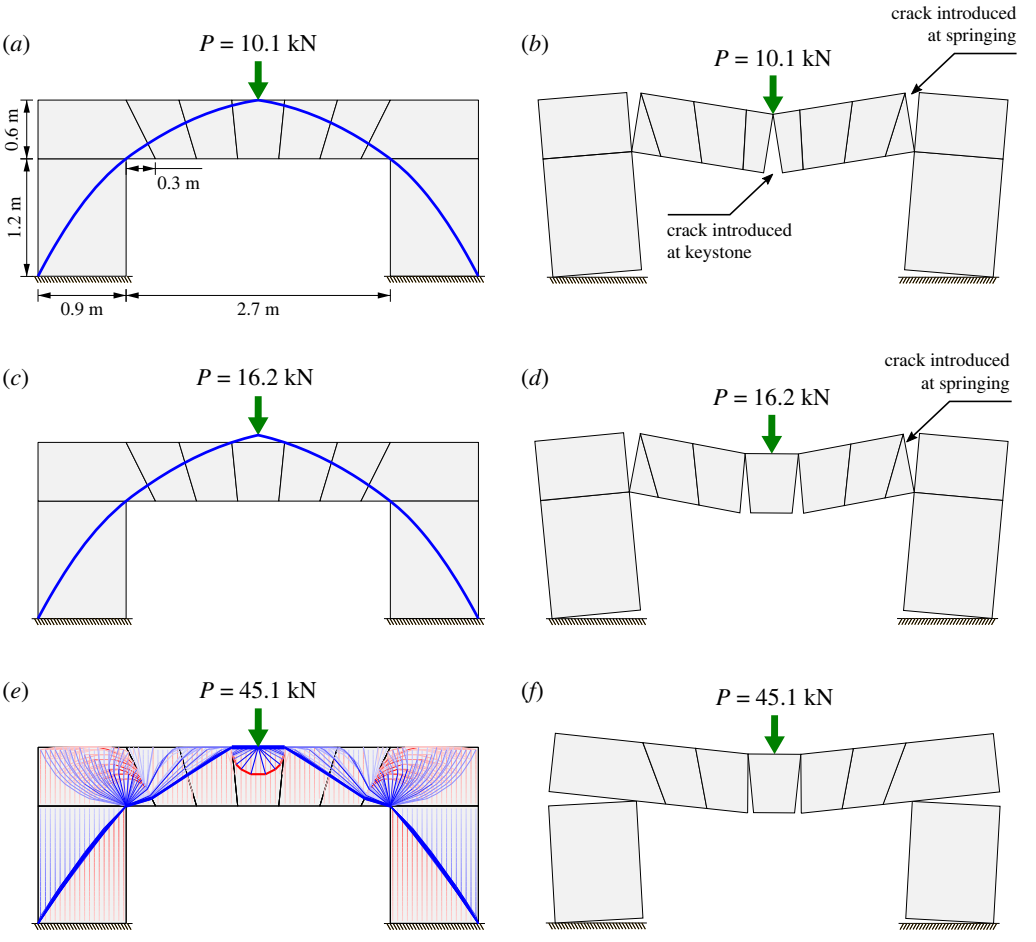

Figure 8. Flat arch on stone columns—solutions obtained via: (*a*) traditional thrust line method; (*b*) rigid block method, after three extra vertical failure planes added; (*c*) thrust line method with thrust constrained at block interfaces only; (*d*) rigid block method, after two extra vertical failure planes added; (*e*) TLO, showing force flows confined to areas where material is present (transmissible self-weight vectors also plotted); (*f*) rigid block method, with no extra failure planes added to provide agreement with TLO solution, since this takes actual block stereotomy into account (all five blocks in the arch have a top breadth of 0.54 m and a bottom breadth of 0.42 m; a width of 1 m and material unit weight of 25 kN m^{-3} are assumed; thrust lines obtained using vertical strips of 0.05 m width; thrust layouts obtained using internal and boundary node spacings of 0.05 and 0.01 m, respectively, and $q^{t}_{max} = 250$ N).

By contrast, when using TLO, weak interfaces are explicitly taken into account, with a limited amount of tension inside blocks permitted as part of the formulation. While the resulting TLO solution (figure 8*e*) includes thick blue lines reminiscent of a traditional thrust line, tensile forces are now also evident in the keystone and springing blocks, providing an indication as to how the self-weight of the latter are mobilized. In the keystone block, the thrust layout resembles the form of the optimal half-wheel truss structure, whereas in each springing block the thrust layout resembles an optimal Michell cantilever truss structure [56]. In addition, transmissible self-weight vectors are also shown in figure 8*e*, making the transmissible load representation of the self-weight of the masonry clear.

It is also of interest to investigate the sensitivity of the TLO solutions for this example to both the selected nodal density and the maximum allowed tensile force, q^{t}_{max}. Thus figure 9 shows how the computed collapse load converges towards the exact value, of $P = 45.1$ kN, as the

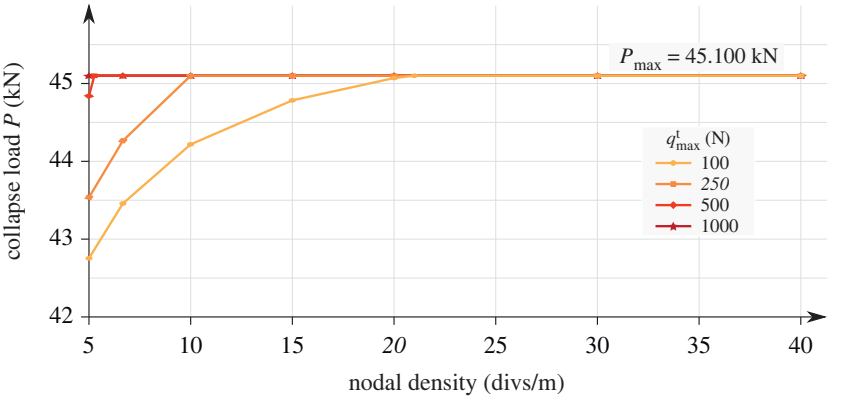

Figure 9. Flat arch on stone columns: computed collapse load versus nodal density for a range of maximum allowed tensile force values, q^t_{max} (quoted nodal density is the reciprocal of the internal node spacing; boundary node spacing is 0.2 × internal node spacing; values in italics used to generate figure 8*e*).

nodal density is increased for a range of values of q^t_{max}. It is evident that for higher q^t_{max} values, convergence occurs at lower nodal densities, with the computed collapse load converging to the exact collapse load at a very low nodal density when $q^t_{max} = 1000$ N.

As an alternative to considering the maximum tensile force, q^t_{max}, the thickness of material required to carry this can instead be considered, calculated assuming the masonry blocks possess finite but low tensile strength, here taken as 1 N mm^{-2}. Thus figure 10 shows how the computed collapse load varies with required stressed thickness, for a range of different nodal densities. It is evident that a very low required stressed thickness of 0.25 mm (equivalent to $q^t_{max} = 250$ N) is required in order for the solution to converge to the exact rigid block collapse load in this case. This stressed thickness is several orders of magnitude smaller than the physical dimensions of the structure, and is well within the limits of what could safely be carried by most stone materials. Also, when even lower maximum stressed thickness values are used (e.g. 10^{-5} mm, equivalent to $q^t_{max} = 0.01$ N) it is evident from figure 10 that the solutions lie in close proximity to the compression-only thrust line solution of figure 8*a*. (Note though that the compression-only TLO solution will at the limit lie below the corresponding thrust line method solution. This is because the transmissibility of the block self-weight is constrained at interfaces when using TLO, such that 'pulling up' the weight of lower blocks to the main part of the thrust line will require a finite, albeit small, tensile capacity.)

Finally, the CPU times required to obtain TLO solutions for a range of nodal densities are summarized in table 1, with the associated number of links and nodal interface pairs also shown. Note that internal nodes are positioned on a Cartesian grid while boundary nodes are uniformly spaced though with extra boundary nodes added to model load transmissibility. It has been observed that although the exact collapse load can be obtained using a coarse nodal density, the use of finer nodal densities often allows the flow of forces to be more clearly visualized, albeit at higher computational cost.

(b) Applications

The TLO method is now applied to two rather more practical masonry structures, namely (i) a two-ring arch, and (ii) a masonry buttress wall.

(i) Two-ring arch

This examples involves a two-ring brickwork arch rib load tested to collapse in the laboratory by Melbourne & Gilbert [28]. The specific arch rib considered here incorporated a continuous sand joint between the two rings of brickwork to replicate a structure in the field with debonded arch

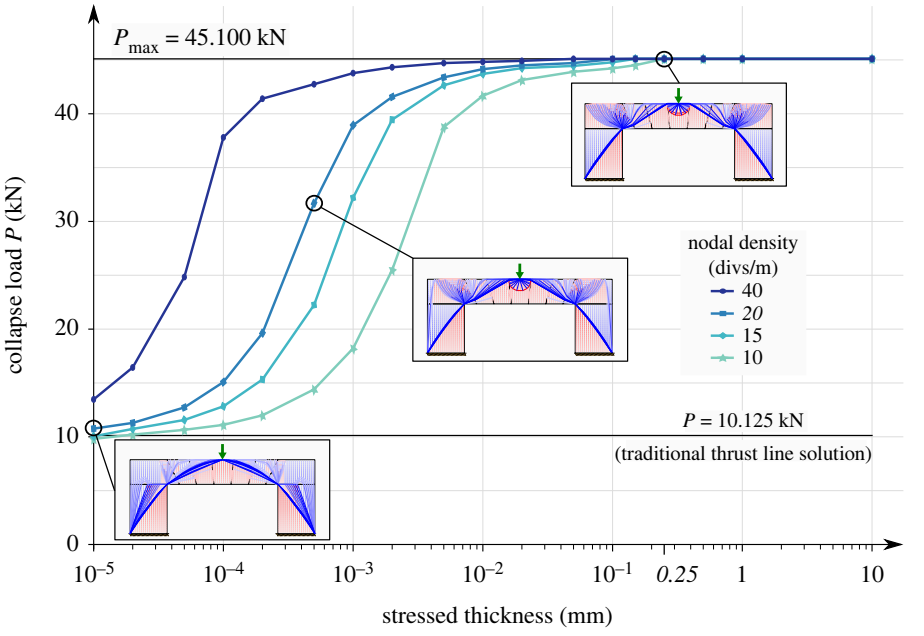

Figure 10. Flat arch on stone columns: computed collapse load versus stressed thickness, for a range of nodal densities (stressed thickness indicated based on an assumed tensile strength of 1 N mm^{-2}; values in italics used to generate figure 8*e*).

Table 1. Flat arch on stone columns: CPU time for solutions at different nodal densities (nodal density with respect to internal nodes; boundary node spacing is ×0.2 internal node spacing; q^{t}_{max} of 250 N ; values in italics used in figure 8*e*).

					CPU time (s)[a]	
nodal density (divs/m)	*nodes*	links	interface pairs	collapse load (kN)	load eval.	vol. min.
5	1091	61 672	264	43.536	0.4	3.1
6.67	1430	106 641	326	44.265	0.6	6.3
10	2261	274 726	470	45.100	2.0	9.9
15	3968	858 443	776	45.100	5.7	24.5
20	*5628*	*1 769 939*	*990*	*45.100*	*15.2*	*48.6*
30	9645	5 465 060	1384	45.100	49.1	122.4
40	15 146	13 713 614	1984	45.100	139.8	476.8

[a]LP time as reported by the solver; load evaluation with full ground-structure; volume minimization with member adding starting with a minimal ground structure—see [57].

rings; see figure 11. The material unit weight was reported to be 23.7 kN m^{-3} and the friction coefficient of the sand joint to be 0.53.

Firstly, considering the traditional thrust line analysis method, to bound the solution from above the arch can be represented by a single 215 mm thick arch ring. Thus, assuming the thrust line is constrained only at weak radial interfaces, the predicted collapse load is 3.79 kN, and the corresponding thrust line solution is shown in figure 12*a*. Alternatively, by constructing a separate thrust line for each arch-ring, the solution can be bounded from below, with the predicted collapse load now 1.15 kN (based on 0.55 kN being carried by the top ring and 0.60 kN carried by the bottom ring, and no interaction between rings), and the corresponding thrust line solution is shown in figure 12*b*.

Figure 11. Two-ring arch—experimental testing: (*a*) initial set-up; (*b*) hinges forming; (*c*) collapse of structure (arch has 3 m span, 0.75 m rise, 215 mm thickness and 215 mm width and is subject to point load 0.84 m from left abutment [28]).

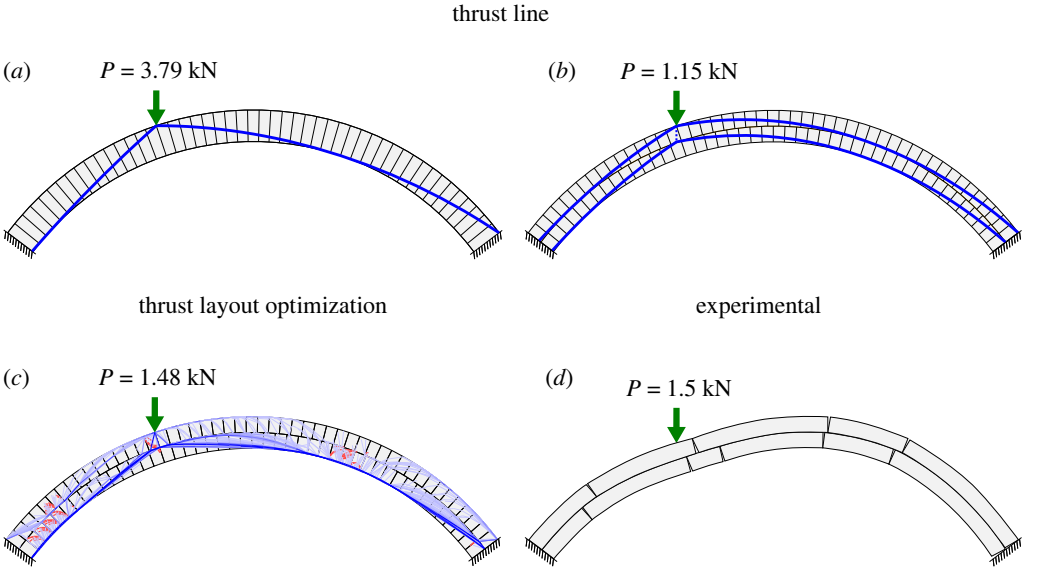

Figure 12. Two-ring arch—solutions obtained via: (*a*) traditional thrust-line method, assuming single monolithic arch ring; (*b*) traditional thrust-line method, determining separate thrust lines for each arch ring; (*c*) TLO, showing associated force flows; (*d*) experimental test, showing observed failure mechanism [28] (thrust lines obtained assuming self-weight lumped at block centroids; thrust layouts obtained using internal and boundary node spacings of 0.01 and 0.005 m, respectively, and $q^{t}_{max} = 1$ N; thrust layout tensile force line thickness scaled by a factor of 2 for emphasis).

By contrast, when using TLO the combined effects of both rings can be modelled directly. The TLO solution for this problem is shown in figure 12*c*, with the corresponding predicted collapse load being 1.48 kN, which closely matches the experimentally obtained value of 1.5 kN [28]. Whereas the thrust line method is able to successfully bracket the experimental value, the upper and lower bound thrust line solutions (3.79 and 1.15 kN) are too far apart to be practically useful.

The TLO solution shown in figure 12*c* also provides an indication as to how the load is being carried, here indicating that the loading is primarily carried by the bottom arch ring, with the main thrust hugging the intrados near the left-hand support and in the three-quarter span region, also touching the extrados of the bottom arch ring directly below the loading point and at the right hand support. These appear broadly in line with the experimentally observed mechanism; see figure 12*d*.

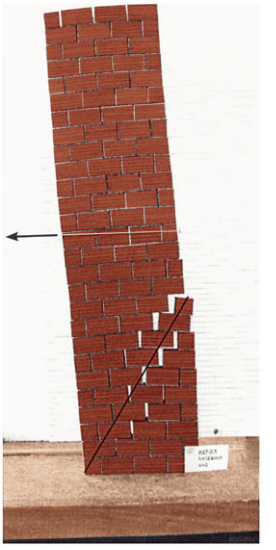

Figure 13. Masonry buttress—horizontal mid-height load test: blocks below diagonal black line deemed ineffective in resisting the load (test carried out by Ochsendorf [58], reproduced here as a colourized image).

(ii) Masonry buttress

When the traditional thrust line method is applied to structures such as leaning towers [24] and buttresses [58] an additional step is generally required in order to identify how much of the masonry will be effective in resisting the applied loading; e.g. see figure 13. A benefit of TLO is that this is not required when the structure is modelled using the appropriate discretization of blocks (size, aspect-ratio and stacking pattern) and friction capacity, since the effective (and ineffective) regions can in this case be identified automatically. Alternatively, were a buttress wall to be modelled as a continuum using TLO then plotting the transmissible self-weight load vectors would likely cause the engineer to quickly question this representation, as the self-weight of sections of the wall being 'lifted up' would be clearly visible. Furthermore, this suggests that only the region of masonry lying below the thrust line would need to be faithfully modelled—and hence also suggests a potential staged approach to modelling, in which the masonry is only modelled in detail in regions where an initial analysis has indicated that this is necessary.

Here, the masonry buttress in figure 14*a* is considered; this has a base width of 0.54 m and a total weight of 19.05 kN, acting along a line of action at a distance of 0.30 m from the left-hand corner. An external load, inclined to the horizontal at an angle $\tan^{-1} 1.25$, is applied at a height of 1.68 m. This loading is representative of the load applied from a flying buttress. The material unit weight is 18 kN m^{-3} and a unit width of buttress is assumed.

Using the traditional thrust line method, a collapse load of 9.04 kN is predicted for the buttress (figure 14*b*), reducing to 6.61 kN if an ineffective area of the structure is assumed (using the method proposed by Ochsendorf [58]; see figure 14*c*). In this example, the fracture line defining the extent of the ineffective area extends to 0.87 m above ground level.

Modelling the structure as a continuum in TLO reproduces the traditional thrust line method collapse load of 9.04 kN, but how the self-weight loading is carried is now clearer (figure 14*d*). Taking account of the masonry bonding pattern but assuming infinite joint friction capacity, the same collapse load of 9.04 kN is predicted via TLO. However, the self-weight load is now mobilized via a different mechanism (figure 14*e*). The inset figure gives a closer view of the flow of forces, which suggest that tensile forces are being transmitted across block interfaces, even though these have been prescribed to be non-tensile resistant; this arises from the frictional resistance of block interfaces. This is also influenced by the aspect ratio of the blocks and the adopted bonding

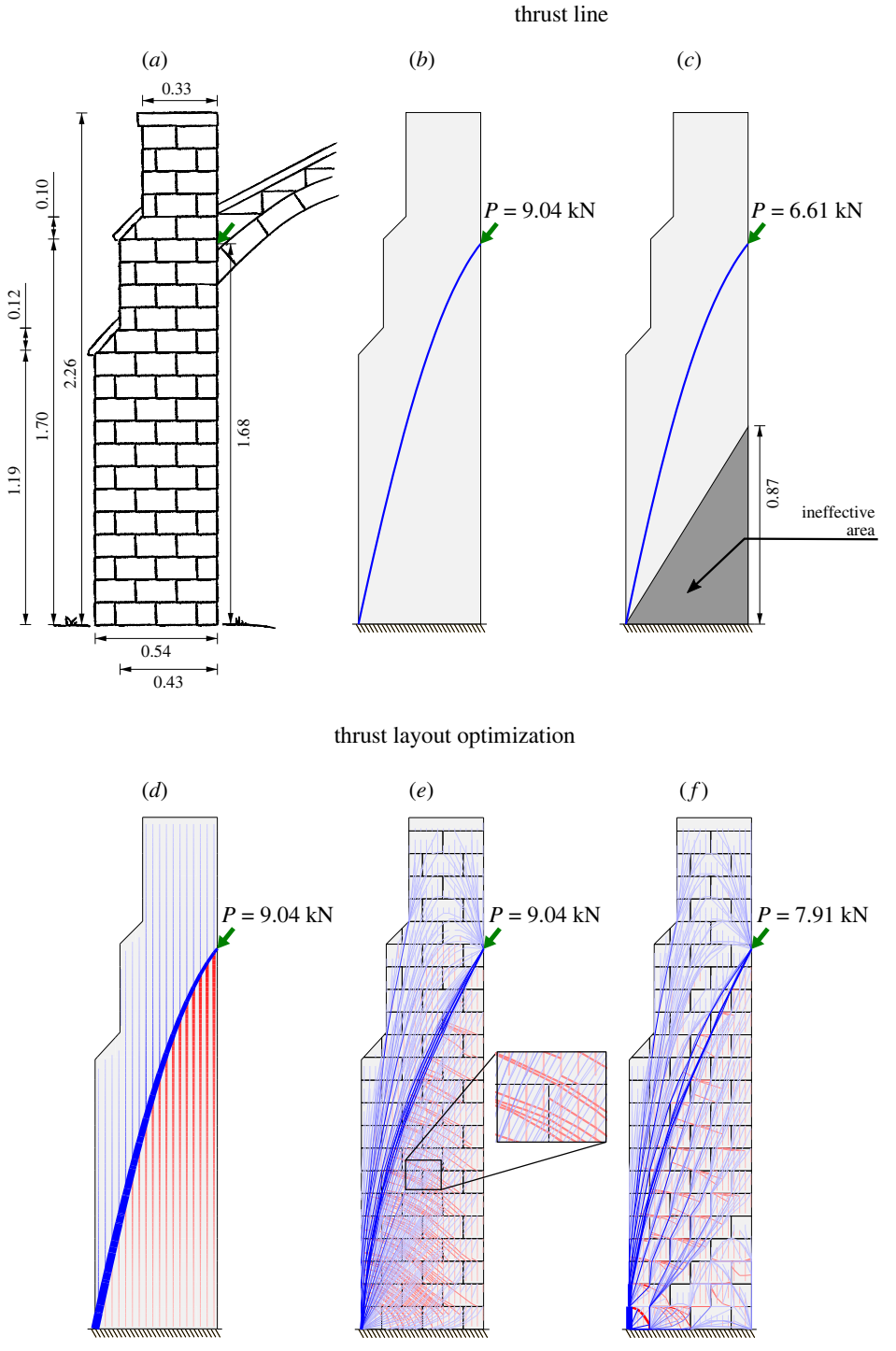

Figure 14. Masonry buttress – geometry shown in (*a*) and assessed using: (*b*) traditional thrust line method; (*c*) traditional thrust line method, considering fracture of the buttress; (*d*) TLO, considering the structure as a continuum, rationalized via a geometry optimization post-processing step and with transmissible load vectors plotted; (*e*) TLO, as a block assembly with infinite friction resistance; (*f*) TLO, as a block assembly with friction limited by a friction coefficient of 0.7 (thrust lines obtained using vertical strips of 0.03 m width; thrust layouts in continuum solution obtained using internal and boundary node spacings of 0.03 m; thrust layouts in block assembly solutions obtained using internal and boundary node spacings of 0.025 and 0.01 m, respectively; $q^{t}_{max} = 150$ N; tensile force line thickness scaled by a factor of 2 for emphasis; links with forces lower than 0.0001 f_{max} not plotted; all dimensions in metres).

(interlocking) pattern, a phenomenon previously investigated by Bacigalupo *et al.* [59], and more recently in [60,61].

When the friction coefficient is set to a realistic value, in this case 0.7, the predicted collapse load reduces to 7.91 kN. The resulting thrust layout in figure 14*f* indicates that the self-weight of several blocks in the bottom-right corner are now not 'lifted up' to the main line of compression that runs from the applied load down to the supports. However, this region is not fully inactive, and does contribute to resisting the applied load. This suggests that the method proposed by Ochsendorf provides a conservative estimate of the load capacity (amounting to 84 % of the TLO solution in this case). This is because it does not consider the tensile strength of the blocks or the bonding pattern, with the degree of underestimation becoming more significant as blocks become larger.

(c) Commentary

In several of the examples considered in this section, it has been demonstrated that frictional (sliding) failures at interfaces between blocks can readily be modelled in the TLO procedure. However, it is worth noting that although the flow rule is not explicitly specified in the TLO formulation presented, the use of a maximization step in the procedure means that the friction is implicitly assumed to be associative (i.e. that any sliding movement will be accompanied by dilation (e.g. [11]), with the angle of dilation equal to the angle of sliding friction, i.e. $\tan^{-1}\mu$). Although this behaviour is not physically realistic, and can lead to overestimates of the safety of a given structure, the degree of any overestimation is likely to be relatively modest when the structure is discretized using a large number of blocks [62]. Also, this issue could potentially be addressed by replacing the single maximization step used in the presented TLO method with an iterative procedure, similar to that proposed for use with rigid block limit analysis by Gilbert *et al.* [14].

Finally, although two-dimensional examples have been used to demonstrate the capability of the TLO procedure, this is in principle readily extendable to three-dimensional problems. The procedure can also potentially be extended to be applicable to retrofit design problems, allowing optimally placed strengthening measures to be identified in existing masonry gravity structures.

4. Conclusions

A new procedure has been developed that allows both the safety of masonry gravity structures to be evaluated and the transmission of internal forces to be clearly visualized. The procedure builds on a truss layout optimization with transmissible loads formulation, using this to model self-weight, and with interfaces included in the formulation to model weak masonry joints. The new procedure is herein termed thrust layout optimization (TLO):

— Although the traditional thrust line analysis method has proved useful for many years, it has some limitations. For example, block stereotomy is not considered, leading to self-weight being 'lifted up' across weak interfaces. Also, unlimited friction capacity is usually assumed, leading to sliding failures not being identified. The TLO procedure overcomes these limitations by considering block stereotomy, the low (but finite) tensile strength of blocks, and the limited friction capacity of interfaces, to furnish the exact collapse load for any given problem. Furthermore, TLO eliminates the need for case specific assumptions, which are very often required when using the traditional thrust line method (e.g. estimating the ineffective area in a buttress wall, or postulating potential load paths in a multi-ring arch).

— The thrust layouts identified via TLO provide a rich visual representation of force flows in masonry gravity structures. The procedure takes on board the limited tensile capacity of masonry blocks and makes no prior assumptions about the topology of thrust layouts. This enables visualization of forces flowing around internal holes, with

the force flows associated with blocks rocking about vertices often resembling classical Michell structures; more familiar funicular thrust line solutions can also be identified. It is also possible to plot transmissible self-weight vectors, eliminating ambiguity as to how self-weight forces are mobilized.

— The TLO procedure thus provides a fully automated means of generating a thrust layout and determining the associated collapse load for any given problem, comprising an arbitrary arrangement of masonry blocks. Computed collapse loads are found to be comparatively insensitive to the chosen numerical discretization (spacing of nodes) and the tensile force allowed within masonry blocks, with exact solutions obtainable at modest computational cost by taking advantage of efficient and widely available LP solvers.

Although a range of sophisticated nonlinear analysis methods are now available for masonry structures, these are generally too demanding of computer time and operator expertise for routine use. This means that there remains a need for simple and intuitive analysis models, which provide clear and reliable results. Since the proposed TLO procedure successfully overcomes a number of the known weaknesses of the traditional thrust line analysis method, it has the potential to form an invaluable part of the tool-sets of engineers responsible for analysing masonry gravity structures.

Data accessibility. A Python script and accompanying data files has been made available to enable the solutions obtained herein via the TLO procedure to be replicated: https://dx.doi.org/10.15131/shef.data.21836541.

Authors' contributions. K.I.U.N.: investigation, methodology, software, validation, visualization, writing—original draft, writing—review and editing; A.L.: conceptualization, methodology, software, supervision, writing—original draft, writing—review and editing; M.G.: conceptualization, funding acquisition, methodology, project administration, supervision, writing—original draft, writing—review and editing.

All authors gave final approval for publication and agreed to be held accountable for the work performed therein.

Conflict of interest declaration. We declare we have no competing interests.

Funding. M.G. acknowledges the financial support provided by the Engineering and Physical Research Council under grant reference no. EP/T001305/1.

Acknowledgements. The authors thank Dr Linwei He for advice and for making available a Python script for rationalizing the generated layout optimization solutions via geometry optimization.

References

1. Kurrer KE. 2008 *The history of the theory of structures: from arch analysis to computational mechanics*. Berlin, Germany: Ernst & Sohn.
2. Roca P, Cervera M, Gariup G, Pela' L. 2010 Structural analysis of masonry historical constructions. Classical and advanced approaches. *Arch. Comput. Methods Eng.* **17**, 299–325. (doi:10.1007/s11831-010-9046-1)
3. Lenczner A. 2020 Speaking stone–a retrospective look at the stone arch design for the Padre Pio Church, Italy. *Struct. Eng.* **98**, 30–39. (doi:10.56330/RVRB7716)
4. Webb S. 2020 Stone rises. *RIBA J.* **127**, 52–54.
5. Graefe R. 2021 The catenary and the line of thrust as a means for shaping arches and vaults. In *Physical Models: their historical and current use in civil and building engineering design* (ed. B Addis), pp. 79–126. Berlin, Germany: Ernst & Sohn.
6. Heyman J. 1982 *The Masonry Arch*. Chichester: Ellis Horwood.
7. Lemos JV. 2007 Discrete element modeling of masonry structures. *Int. J. Archit. Herit.* **1**, 190–213. (doi:10.1080/15583050601176868)
8. Beatini V, Royer-Carfagni G, Tasora A. 2017 A regularized non-smooth contact dynamics approach for architectural masonry structures. *Comput. Struct.* **187**, 88–100. (doi:10.1016/j.compstruc.2017.02.002)
9. Kooharian A. 1952 Limit analysis of voussoir (segmental) and concrete arches. *J. Am. Conc. Inst.* **24**, 317–328.
10. Heyman J. 1966 The stone skeleton. *Int. J. Solids Struct.* **2**, 249–279. (doi:10.1016/0020-7683(66)90018-7)

11. Livesley RK. 1978 Limit analysis of structures formed from rigid blocks. *Int. J. Numer. Methods Eng.* **12**, 1853–1871. (doi:10.1002/nme.1620121207)
12. Ferris M, Tin-Loi F. 2001 Limit analysis of frictional block assemblies as a mathematical program with complementarity constraints. *Int. J. Mech. Sci.* **43**, 209–224. (doi:10.1016/S0020-7403(99)00111-3)
13. Orduña A, Lourenço PB. 2003 Cap model for limit analysis and strengthening of masonry structures. *J. Struct. Eng.* **129**, 1367–1375. (doi:10.1061/(ASCE)0733-9445(2003)129:10(1367))
14. Gilbert M, Casapulla C, Ahmed HM. 2006 Limit analysis of masonry block structures with non-associative frictional joints using linear programming. *Comput. Struct.* **84**, 873–887. (doi:10.1016/j.compstruc.2006.02.005)
15. Nodargi NA, Intrigila C, Bisegna P. 2019 A variational-based fixed-point algorithm for the limit analysis of dry-masonry block structures with non-associative Coulomb friction. *Int. J. Mech. Sci.* **161–162**, 105078. (doi:10.1016/j.ijmecsci.2019.105078)
16. Gilbert M. 1997 Gross displacement mechanism analysis of masonry bridges and tunnel linings. In *Proc. 11th Int. Brick Block Mason. Conf., Shanghai, China, 14–16 October*, pp. 473–482.
17. Iannuzzo A, Dell'Endice A, Van Mele T, Block P. 2021 Numerical limit analysis-based modelling of masonry structures subjected to large displacements. *Comput. Struct.* **242**, 106372. (doi:10.1016/j.compstruc.2020.106372)
18. Casapulla C, Portioli F, Maione A, Landolfo R. 2013 A macro-block model for in-plane loaded masonry walls with non-associative Coulomb friction. *Meccanica* **48**, 2107–2126. (doi:10.1007/s11012-013-9728-5)
19. O'Dwyer D. 1999 Funicular analysis of masonry vaults. *Comput. Struct.* **73**, 187–197. (doi:10.1016/S0045-7949(98)00279-X)
20. Block P, Ochsendorf J. 2007 Thrust network analysis: a new methodology for three-dimensional equilibrium. *J. Int. Assoc. Shell Spat. Struct.* **48**, 167–173.
21. Maia Avelino R, Iannuzzo A, Van Mele T, Block P. 2021 Assessing the safety of vaulted masonry structures using thrust network analysis. *Comput. Struct.* **257**, 106647. (doi:10.1016/j.compstruc.2021.106647)
22. Huerta S. 2010 The safety of masonry buttresses. *Proc. Inst. Civ. Eng. Eng. Hist. Herit.* **163**, 3–24. (doi:10.1680/ehah.2010.163.1.3)
23. Ochsendorf JA. 2006 The masonry arch on spreading supports. *Struct. Eng.* **84**, 29–35.
24. Heyman J. 1992 Leaning towers. *Meccanica* **27**, 153–159. (doi:10.1007/BF00430041)
25. Heyman J. 2009 La coupe des pierres. In *Proc. 3rd Int. Congr. Constr. Hist., Cottbus, Germany, 20–24 May* (eds KE Kurrer, W Lorenz, V Wetzk), pp. 807–812.
26. Nikolinakou MK, Tallon AJ, Ochsendorf JA. 2010 Structure and form of early Gothic flying buttresses. *Eur. J. Environ. Civ. Eng.* **9**, 1191–1217. (doi:10.1080/17747120.2005.9692807)
27. Fuentes P. 2018 Mechanics of flying buttresses: the case of the cathedral of Mallorca. *J. Mech. Mater. Struct.* **13**, 617–630. (doi:10.2140/jomms.2018.13.617)
28. Melbourne C, Gilbert M. 1995 The behaviour of multiring brickwork arch bridges. *Struct. Eng.* **73**, 39–47.
29. Xia Y, Langelaar M, Hendriks MAN. 2020 A critical evaluation of topology optimization results for strut-and-tie modeling of reinforced concrete. *Comput. Aided Civ. Infrastruct. Eng.* **35**, 850–869. (doi:10.1111/mice.12537)
30. Milani G, Bruggi M. 2018 Simple homogenization-topology optimization approach for the pushover analysis of masonry walls. *Int. J. Archit. Herit.* **12**, 395–408. (doi:10.1080/15583058.2017.1323248)
31. Dorn WS, Gomory RE, Greenberg HJ. 1964 Automatic design of optimal structures. *J. Mec.* **3**, 25–52.
32. Gilbert M, Tyas A. 2003 Layout optimization of large-scale pin-jointed frames. *Eng. Comput.* **20**, 1044–1064. (doi:10.1108/02644400310503017)
33. Darwich W, Gilbert M, Tyas A. 2010 Optimum structure to carry a uniform load between pinned supports. *Struct. Multidisc. Optim.* **42**, 33–42. (doi:10.1007/s00158-009-0467-0)
34. Lu H, Tyas A, Gilbert M, Pichugin AV. 2021 On transmissible load formulations in topology optimization. *Struct. Multidiscip. Optim.* **64**, 23–37. (doi:10.1007/s00158-021-02932-0)
35. Pritchard T, Gilbert M, Tyas A. 2005 Plastic layout optimization of large-scale frameworks subject to multiple load cases, member self-weight and with joint length penalties. In *Proc. 6th World Congr. Struct. Multidiscip. Optim., Rio de Janeiro, Brazil, 30 May–3 June*.
36. Zegard T, Paulino GH. 2014 GRAND–Ground structure based topology optimization for arbitrary 2D domains using MATLAB. *Struct. Multidiscip. Optim.* **50**, 861–882. (doi:10.1007/s00158-014-1085-z)

37. Sokół T. 2011 A 99 line code for discretized Michell truss optimization written in Mathematica. *Struct. Multidiscip. Optim.* **43**, 181–190. (doi:10.1007/s00158-010-0557-z)
38. Fuchs MB, Moses E. 2000 Optimal structural topologies with transmissible loads. *Struct. Multidiscip. Optim.* **19**, 263–273. (doi:10.1007/s001580050123)
39. He L, Gilbert M. 2015 Rationalization of trusses generated via layout optimization. *Struct. Multidiscip. Optim.* **52**, 677–694. (doi:10.1007/s00158-015-1260-x)
40. Robert McNeel and Associates. 2020 *Rhinoceros: modeling tools for designers (version 6.0)*. [Computer software].
41. Van Rossum G. Python software foundation. 2021 *Python (version 3.7)*. [Computer software].
42. Van Der Walt S, Colbert C, Varoquaux G. 2011 The NumPy array: a structure for efficient numerical computation. *Comput. Sci. Eng.* **13**, 22–30. (doi:10.1109/MCSE.2011.37)
43. Gillies S. 2021 *Shapely (version 1.7.0)*. [Computer software].
44. MOSEK ApS. 2021 *MOSEK Fusion API for Python (version 9.1.8)*. [Computer software].
45. Botsch M, Steinberg S, Bischoff S, Kobbelt L. 2002 Openmesh-a generic and efficient polygon mesh data structure. In *OpenSG Symp*. Darmstadt, Germany.
46. Hagberg AA, Schult DA, Swart PJ. 2008 Exploring network structure, dynamics, and function using NetworkX. In *Proc. 7th Python Sci. Conf. (SciPy2008), Pasadena, CA, 19–24 August* (eds G Varoquaux, T Vaught, J Millman), pp. 11–15.
47. LimitState Ltd. 2021 *LimitState:GEO (version 3.5.g)*. [Computer software].
48. Smith C, Gilbert M. 2007 Application of discontinuity layout optimization to plane plasticity problems. *Proc. R. Soc. A* **463**, 2461–2484. (doi:10.1098/rspa.2006.1788)
49. Gilbert M, Smith CC, Pritchard TJ. 2010 Masonry arch analysis using discontinuity layout optimisation. *Proc. Inst. Civ. Eng. - Eng. Comput. Mech.* **163**, 155–166. (doi:10.1680/eacm.2010.163.3.155)
50. Heyman J. 2010 Equilibrium of masonry arches. *Proc. Inst. Civ. Eng. - Eng. Comput. Mech.* **163**, 129–133. (doi:10.1680/eacm.2010.163.3.129)
51. Alexakis H, Makris N. 2015 Limit equilibrium analysis of masonry arches. *Arch. Appl. Mech.* **85**, 1363–1381. (doi:10.1007/s00419-014-0963-6)
52. Milankovitch M. 1907 Theorie der Druckkurven. *Zeitschrift für Mathematik und Physik* **55**, 1–27.
53. Foce F. 2007 Milankovitch's Theorie der Druckkurven: good mechanics for masonry architecture. *Nexus Netw. J.* **9**, 185–210. (doi:10.1007/s00004-007-0039-9)
54. Nodargi NA, Bisegna P. 2020 A unifying computational approach for the lower-bound limit analysis of systems of masonry arches and buttresses. *Eng. Struct.* **221**, 110999. (doi:10.1016/j.engstruct.2020.110999)
55. Barsi F, Barsotti R, Bennati S, Ciblac T. 2022 Investigating the relation between thrust networks and thrust surfaces for masonry domes subjected to vertical loads: a case study. *Int. J. Archit. Herit.* 1–19. (doi:10.1080/15583058.2022.2101159)
56. Lewiński T, Sokół T, Graczykowski C. 2018 *Michell structures*. New York, NY: Springer.
57. He L, Gilbert M, Song X. 2019 A Python script for adaptive layout optimization of trusses. *Struct. Multidiscip. Optim.* **60**, 835–847. (doi:10.1007/s00158-019-02226-6)
58. Ochsendorf J. 2002 *Collapse of masonry structures*. PhD thesis, University of Cambridge, Cambridge, UK.
59. Bacigalupo A, Cavicchi A, Gambarotta L. 2012 A simplified evaluation of the influence of the bond pattern on the brickwork limit strength. *Adv. Mater. Res.* **368**, 3495–3508. (doi:10.4028/www.scientific.net/AMR.368-373.3495)
60. Beatini V, Royer-Carfagni G, Tasora A. 2018 The role of frictional contact of constituent blocks on the stability of masonry domes. *Proc. R. Soc. A* **474**, 20170740. (doi:10.1098/rspa.2017.0740)
61. Chen S, Bagi K. 2020 Crosswise tensile resistance of masonry patterns due to contact friction. *Proc. R. Soc. A* **476**, 20200439. (doi:10.1098/rspa.2020.0439)
62. Valentino J, Gilbert M, Gueguin M, Smith CC. 2023 Limit analysis of masonry walls using discontinuity layout optimization and homogenization. *Int. J. Numer. Methods Eng.* **124**, 358–381. (doi:10.1002/nme.7124)